# Voxel Based Three-Dimensional Topology Optimization of Heat Exchanger Fins

Bashir S. Mekki<sup>1</sup>, and Stephen P. Lynch<sup>2</sup> The Pennsylvania State University, University Park, PA, 16802

Increasing interest in novel aircraft propulsion systems and potential for unwanted heat generation, or capture and reuse of waste heat, may require increasingly lightweight and high performing heat exchangers. Advances in manufacturing technologies have shown potential to create complex designs, but design tools need more flexibility. This study utilizes genetic algorithm-driven topology optimization to develop high performance heat exchanger fins for critical applications such as aerospace. The solid domain is generated using voxel representation where a voxel value of 1 indicates the solid domain and a voxel value of 0 refers to the fluid domain. The use of voxel representation somewhat matches the digitization of a model that is required to fabricate using additive manufacturing, and also allows for a highly unconstrained geometry. To test the topology optimization approach, a three-dimensional (3D) baseline offset strip fin geometry in steady laminar flow (Reynolds number = 215) with conjugate heat transfer (simultaneous solution of solid and fluid temperature fields) is optimized. New designs are generated using the genetic algorithm (GA) and sent to evaluation by the CFD software OpenFOAM; then the GA sorts and selects the reproduction pool for the following generation. This process is repeated for 60 generations. The study also investigates the effect of fin material on the performance of the GA and the resulting designs. The results show that the optimal designs have overall performance improvement of 18% relative to the baseline. Additionally, a fin constructed of a lower conductivity material (such as an Inconel superalloy that might be necessary for waste heat recovery applications) results in lower overall performance improvement (11%) and optimal designs with higher pressure drop relative to their baseline, and relative to optimal designs produced using higher conductivity materials.

Key words: 3D Optimization, Voxel Based Design, Heat Exchangers, Pressure Drop, Heat Transfer, Topology Optimization, Genetic Algorithm, CFD, Conjugate Heat Transfer, Additive Manufacturing.

## I. Nomenclature

A = cross-sectional area (m<sup>2</sup>)

As = heat transfer surface area  $(m^2)$ 

Cp = specific heat, or static pressure coefficient =  $\frac{dP}{0.5o(\text{Uin})^2}$ 

 $D_h = \text{hydraulic diameter, } D_h = \frac{2(t*Lf)}{(t+Lf)}$ 

dP = pressure drop

dPb= pressure drop from the baseline fin

F = fitness function

Fb = baseline fitness

f = average Fanning friction factor in the offset strip fin array,  $f = \tau_w/(0.5\rho(U_{in})^2)$ 

h = height of the offset strip fin channel, or heat transfer coefficient

i = initial population

 $j = \text{Colburn factor } [j = \text{St Pr}^{2/3} \text{ or Nu/(Re Pr}^{1/3})]$ 

L = material thickness

 $L_f$  = length of fin

 $L_d$  = length of fluid domain

N = number of generations

n = population size of one generation

m = mass flow rate (kg/s)

Nu = average overall Nusselt number based on hydraulic diameter

<sup>&</sup>lt;sup>1</sup> PhD Candidate, Mechanical Engineering, AIAA Member

<sup>&</sup>lt;sup>2</sup> Associate Professor, Mechanical Engineering, AIAA Associate Fellow

P = static pressure

Pr = Prandtl number

Qb = overall heat transfer from the baseline fin

Q = heat transfer rate per unit area (W/m<sup>2</sup>), given by Q = m\*Cp\*(Ts - Tin)

Re = Reynolds number St = Stanton number

s = lateral fin spacing

T = temperature in Kelvin (K)

Ts = wall temperature

Tin= Temperature at the inlet of the fluid domain

t = fin thickness

U<sub>in</sub>= velocity at the inlet of fluid domain

u = x-component of velocity
 v = y-component of velocity
 Z = width of fluid domain
 z = distance along the z-axis

#### **Greek Symbols**

 $\theta$  = nondimensional temperature,  $\theta = \frac{Ts - T}{Ts - Tin}$ 

#### **Abbreviations**

2D = two-dimensional 3D = three-dimensional AM = additive manufacturing CFD = computational fluid dynamic

GA = genetic algorithms HEX = heat exchanger

IMaxM = initial maximum mutation IMinM= initial minimum mutation

OSF = offset strip fin TO = topology optimization

## **II.** Introduction

Heat exchangers (HEXs) can be classified based on flow configuration to co-flow, counter flow, and crossflow. Sub-categories of these classifications include shell and tube heat exchangers, double pipe heat exchangers, plate heat exchangers, condensers, evaporators, and boilers. Of interest to this study are what is commonly known as compact heat exchangers. Compact heat exchangers have a high area density (high surface area to volume ratio). Generally, a compact heat exchange surface is defined as one that has an area density greater than 700 m<sup>2</sup>/m<sup>3</sup> (213 ft<sup>2</sup> / ft<sup>3</sup>). Examples of compact heat exchangers are finned tubes, plate-fin heat exchangers, and microchannel heat exchangers.

Compact heat exchangers are widely used in aerospace applications where the need for lightweight, space saving heat exchangers is very critical. Thermal management systems for aircraft are becoming a major engineering challenge for a variety of aerospace applications. Initial concept studies of hybrid electric aircraft have indicated significant possible efficiency gains and emissions reductions by coupling a traditional fuel-based powerplant with electric components, but more detailed design studies are finding that the additional subsystems required to dissipate heat from electric motors could add up to 1000 lbs. to the airplane and almost negate all benefits of hybrid-electric operation [1]. For military aircraft, weapons systems are requiring more significant electrical power (up to 1000 kW) [2] which generates heat that must be dissipated in a way that does not increase the detectability of the aircraft by enemies. In both of these applications, thermal management is defined as the approach to transfer heat produced in the aircraft, to locations where it can be dissipated. Obviously, it is desirable that this be as lightweight and non-obtrusive as possible. A critically important component of a thermal management system is a heat exchanger, which transfers heat from a source (electric motor, laser weapon) to a sink (air, or even aircraft fuel).

Current heat exchanger design is generally restricted to geometries that have well known performance characteristics (pressure drop, heat transfer), where the geometries are very often limited by manufacturability. This also implies a limited ability to integrate the thermal management system closely to the aircraft. Advancement in additive manufacturing allowed for the use of design tools such as topology optimization (TO) to design highly complex heat exchangers and thermo-fluid equipment. This paper attempts to significantly broaden our ability to

generate novel geometries using evolutionary TO methods, in concert with computational fluid dynamics (CFD), and advanced manufacturing capabilities, to enable highly integrated heat exchanger designs.

The main objective of this paper is to introduce a three dimensional (3D) voxel-based topology optimization approach for heat exchanger fins. The conjugate heat transfer problem is considered for more realistic representation of solid-fluid-thermal interaction in the domain. A previous 2D study by the authors [3] has validated the concept of coupling GA-based TO with CFD to produce organic high performance fin designs. In the previous 2D study, a rectangular fin geometry was used as a baseline from which new designs were generated using the GA through the concept of voxel mutation. This is a simple configuration and unrealistic for full heat exchanger applications but enabled testing of the approach with minimal computational resources. Three-dimensional optimization creates a more realistic representation of a heat exchanger and tests the design flexibility of the genetic algorithm but does introduce more design freedom (higher dimensionality of the optimization). In 2D, the number of pixels that can be turned on/off (mutated) is limited. Expanding the domain to 3D increases the number of voxels that can be mutated by orders of magnitude. This is expected to result in better performing designs since the GA now has a larger domain that allows for unique combinations. A 3D solid-fluid domain with two rectangular baseline fins arranged in an offset strip fin (OSF) configuration with conjugate heat transfer boundary conditions and laminar flow regime is used.

The study also aims to understand the effect of fin material type on the performance of GA and the resulting designs. There are many available materials that can be used for heat exchangers depending on the targeted application. There are many factors that influence the selection process such as cost, weight, thermal efficiency, durability, and corrosion resistance. For example, in ground applications such as industrial and power plants, cost typically plays a more important role than size and weight restrictions. Thus a low-cost material is selected over a potentially more expensive material with higher thermal performance [4]. In aerospace applications on the other hand, the weight and size restrictions, and the high performance requirements are much more important factors than the cost [5].

#### III. Previous Studies

The advent of additive manufacturing (AM) provided more flexibility to design heat exchangers. Researchers are able to design and manufacture complex fin shapes and full-size heat exchangers and other thermal-fluid equipment (heat sinks). Saltzman et al. [6] used AM to create an aircraft oil cooler heat exchanger and experimentally compared its performance to a traditionally manufactured one of similar geometry. Their results showed that the additively manufactured HEX (as is, no postprocessing) has a 10% heat transfer performance improvement over the traditional HEX, however, this comes with the expense of added pressure drop. They noted that the enhanced heat transfer performance is due to the roughness associated with AM. This study demonstrates AM capability to produce fully functioning heat exchangers for real life applications. Wong et al. [7] additively manufactured heat sinks with unique and uncommon geometries which demonstrated AM potential for building unique and creative designs. Advancement in AM has encouraged researchers to design more complex shapes using tools such as topology optimization.

Topology optimization (TO) is mainly used in the field of structural optimization to design mechanical parts in which it is desired to reduce the material without compromising the mechanical strength of the parts. TO was introduced by Bensoe and Kikuchi in 1988 [8]. Since then, it has been expanded to many other applications including the design of thermo-fluid equipment such as heat exchangers. Generally, TO approaches can be classified into gradient based and non-gradient-based methods. Gradient-based methods (level set, density, phase field) [9–13], also known as non-evolutionary methods, use mathematical programing techniques such as the method of moving asymptotes, and the optimal criteria algorithm. Non-gradient methods (also known as evolutionary methods) such as genetic algorithm and simulated annealing rely on heuristic approaches to navigate the design space.

Most TO studies focused on the design of thermo-fluid equipment such as HEX have used gradient based approaches. Hoghoj et al. [14] used density based topology optimization method to optimize a HEX with two fluids. The objective was to maximize the heat transfer while maintaining a fixed pressure drop value. A 2D domain was used to validate the methodology which was then tested on a 3D shell-and-tube case. The results showed that the full freedom topology optimization approach is shown to yield performance improvements over the baseline of up to 113% under the same pressure drop. Feppon et al. [15] optimized three-dimensional fluid-thermal-structural systems. They performed shape and topology optimization using the methods of Hadamard and modified level set, respectively. The developed method is tested on true multiphysics cases represented by fluid-structure interaction, and convective heat transfer. They found that remeshing explicitly the fluid-solid interface at every iteration with a locally high resolution allowed them to obtain very original designs which could have been difficult to capture with more classical methods relying on fixed meshes.

Gradient-based TO methods used for the design of heat exchangers and other complex thermo-fluids equipment are generally based on parametric definition of small to moderate number of constraints, so that the change of the

objective function with a change in the design parameter (gradient) can be simply evaluated and the optimization can be fast. However, they have some major drawbacks [16]:

- They can easily get trapped in local optima and are therefore highly sensitive to the provided starting point, especially when strongly nonlinear systems are studied.
- They can easily become computationally prohibitive as the number of design parameters increases because they require evaluating the gradient at each instance.
- Their efficiency is severely challenged in situations where the objective function exhibits discontinuities (discrete problems) or is strongly non-linear.

Evolutionary methods [17–19], such as genetic algorithms are not required to have parametric constraints unless desired by the design problem. All solutions in a population are searched simultaneously, which greatly decreases the probability that the algorithm is trapped in a local optimal solution [20]. They can have a broader search space but can take more computational resources to evaluate candidate designs.

The bulk of the studies utilized GA for the design of HEX have focused on parametric optimization of fin dimensions (height, width, thickness, pitch, etc.) to meet certain criteria of pressure drop and heat transfer [21–23]. Obviously, parametric optimization approach does not fully take advantage of the GA ability to optimize a large number of degrees of freedoms to produce freeform designs that are far better performing than parametrized designs. For this reason, a previous study by the authors [3] successfully coupled GA with CFD and produced organic designs that have at least 45% performance improvement over a rectangular baseline design. The GA was given the freedom to generate freeform designs, and the only dimensional constraint was the total volume of the solid-fluid domain. Furthermore, of the few papers that utilized GA for HEX design, only a limited number of them have considered the three-dimensionality of the problem. The proposed study aims to optimize the fin shapes in 3D using the methods articulated in [3]. The three-dimensionality will also provide a more realistic understanding of flow physics. In addition to understanding the effect of three-dimensionality on the performance of the resulting designs, this study also investigates the effect of different fin materials on the performance of the GA and the resulting fin shapes.

# IV. Modeling and Optimization Methodology

The modeling and optimization process consists of two parts: generation of new designs using the GA, and evaluation of generated designs using CFD. First, to allow for a significant parameter space, a 3D rectangular shaped baseline fin geometry with two rows of fins arranged in an offset strip fins setting (OSF) is created using voxel representation, where a voxel in the design space is denoted as solid or fluid and can be switched from one to the other by the optimization software. To generate optimal designs, an initial population is generated by mutating the baseline fin a random number of times between the Initial Minimum Mutation (IMinM) and Initial Maximum Mutation (IMM). The population members are then each evaluated in a 3D CFD simulation in OpenFOAM to calculate the performance of each design, as determined by pressure drop and heat transfer. The genetic algorithm is applied to select best designs, merge them (reproduction), and apply random mutations to generate a new generation. The new generation is re-evaluated in CFD for performance, and the process is repeated for a sufficient number of generations to achieve optimal performance. These steps are summarized in **Fig. 1** (adopted from previous 2D study) which describes the overall CFD-GA approach used here. The process is executed in a Python code with embedded functions that communicate with the CFD evaluation software, and has been validated using the 2D study[3].

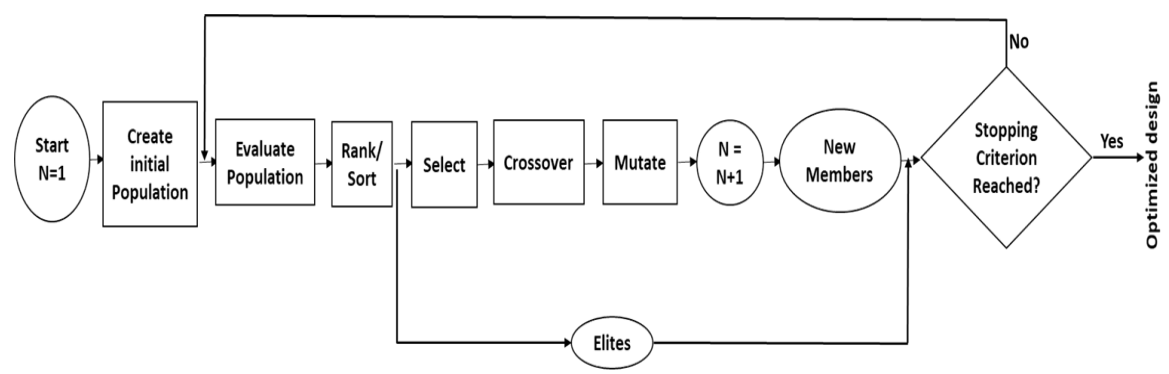


Fig. 1 Overall optimization process workflow [3].

The size and shape of the fluid domain remains the same for each fin while the fin dimensions are allowed to change to any size within the domain. The fluid domain is chosen to be 17.5mm in length (x-direction), 5mm in height

(y-direction), and 3mm in width (z-direction). Each fluid domain is simulated using a structured mesh with equal cell sizes. The domain is meant to simulate a two fin unit in a plate fin heat exchanger similar to those used as oil coolers in small airplanes[24]. **Fig. 2** shows the domain of the baseline geometry along with boundary conditions. The periodic boundary shown allows the simulation to act as an infinitely wide array of fins in the traverse direction with fin spacing of 3mm. The flow is not periodic in the streamwise direction for the purpose of simplicity. For a closer representation of an actual HEX, conjugate heat transfer is simulated by setting the top and bottom surfaces of the domain, including the ends of the fin surfaces, to a constant surface temperature of 450K. Fourier's conduction equation is solved to obtain the temperature field inside the fins. Fluid properties are set to be temperature dependent, using OpenFOAM polynomial transport model [25]. The incoming fluid is at a uniform temperature of 300K and inlet velocity of 2 m/s (Re\_Dh= 223). **Table 1** provides a summary of the boundary conditions.

The fluid solver is chtMultiRegionSimpleFoam, which is a steady-state solver for buoyant, turbulent fluid flow and solid heat conduction with conjugate heat transfer between solid and fluid region. A laminar model is used with a Gauss linear gradient scheme for pressure and Bounded Gauss Upwind divergence scheme for all field variables. The Semi-implicit Method for Pressure-linked Equations (SIMPLE) algorithms have been employed to solve for velocity and pressure equations. A Geometric agglomerated Algebraic MultiGrid (GAMG) solver with Diagonal incomplete-Cholesky (DIC) preconditioner is used to solve for pressure while a Stabilized Preconditioned Bi-Conjugate Gradient (PBiCGStab) solver with Diagonal incomplete-LU (DILU) preconditioner is used to solve for the rest of the field variables. The solution is deemed converged if all the residuals fall under a tolerance value of  $10^{-6}$  or stop changing over 10 iterations.

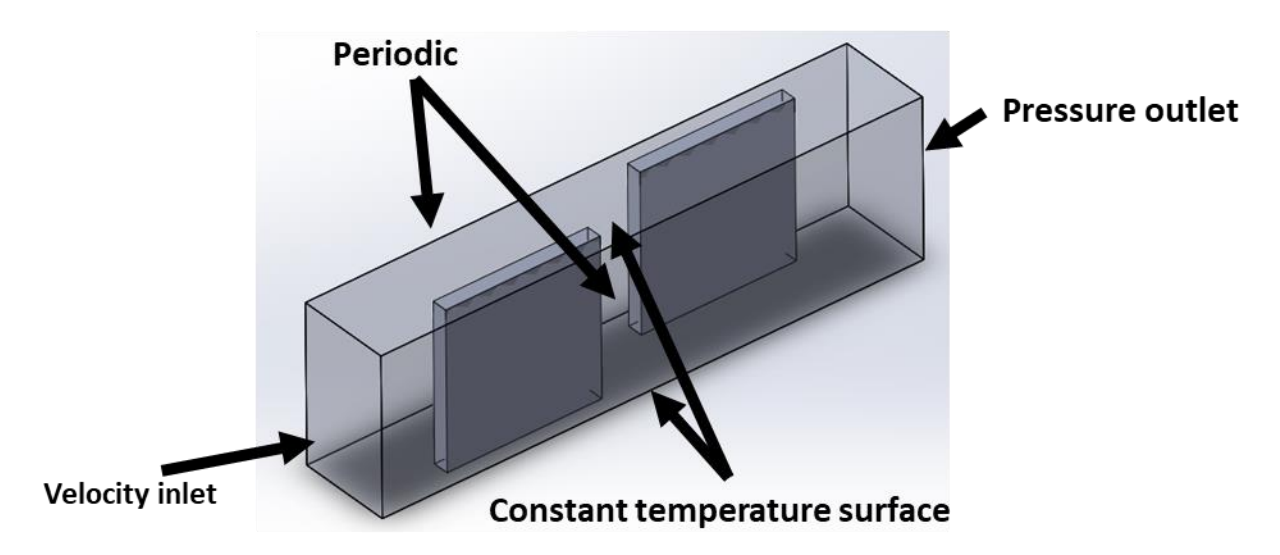


Fig. 2 The baseline geometry used for 3D optimization along with boundary conditions.

Table 1: summary of domain boundary conditions

Location	Boundary type	Flow condition	Thermal condition
Inlet	Velocity inlet	Laminar @ 2m/s	T = 300K
Outlet	Pressure outlet	Laminar	T = 300K
Front & back	Periodic	Periodic	Periodic
Top – fluid & fins	Constant temperature wall	No slip	T = 450K
Bottom – fluid & fins	Constant temperature wall	No slip	T = 450K

# A. CFD Grid Study

OpenFOAM was chosen to perform the optimization because of an easy linkage with the GA code through the Python programming language. This allows for the automation of the entire process and seamless transmission of the new design geometries. As pointed out in [3], there are no published results known to the authors that provide heat transfer and pressure drop for only two rows of fins arranged in an offset strip fashion. For this reason, the baseline geometry in Fig. 2 is simulated in ANSYS Fluent and the results are used as a benchmark to check the validity of the results obtained by OpenFOAM. This enabled the determination of the minimum mesh size in OpenFOAM required

to properly capture gradients. Note that the flow regime considered here is restricted to laminar so the governing equations for the fluid domain are straightforward, without assumptions about an eddy viscosity.

Four mesh sizes (60000, 120000, 250000, 500000 cells) were considered in OpenFOAM and Fluent and the field parameters of interest, the overall heat transfer rate and the overall pressure coefficient are calculated and compared for each mesh. The overall heat transfer used in the GA fitness function is calculated using the mass averaged temperature at the outlet of the domain. The static pressure coefficient is calculated using the definition provided in the nomenclature section in which the pressure drop (dP) is evaluated through the difference in average inlet and outlet pressure. Fig. 3a and b respectively shows the total heat transfer from the solid-fluid domain and the pressure coefficient for every Fluent and OpenFOAM mesh. In Fig. 3a the Fluent and OpenFOAM meshes show a good agreement for a given solver, but the OpenFOAM meshes predicted slightly higher values with a maximum of 10% (0.23W) difference for the 500k mesh. The overall pressure coefficient in Fig. 3b shows the best agreement in the meshes among each other and between the two solvers.

The absence of wall resolved meshing in OpenFOAM implementation is the main reason for the variation observed in Fig. 3. Fluent and OpenFOAM meshes are equal in size, but for purpose of simplicity in the voxel-based design tool, OpenFOAM meshes are simple structured meshes with equal cell size and no clustering. Also, some slight differences might be as to how the solvers are set up, such as convection divergence term schemes (bounded Gauss upwind in OpenFOAM vs Least Squares Cell Based in Fluent). Since the focus of this study is to generate unique designs by combining GA with CFD, the lowest mesh size has been chosen. This allows for shorter calculation times and reasonable accuracy of physics. Fig. 4 shows the CPU and clock time used per simulation for each mesh size in OpenFOAM. It demonstrates the large time savings gained by considering the smallest mesh presented here. The CPU execution time is calculated by running each simulation on the same machine using a single core and same memory characterization. It should be noted that the actual simulation time (clock time) for each case is longer than the CPU execution time when running the coupled GA and CFD code due to the GA steps, and it could vary significantly if the mesh size is larger than the smallest mesh chosen, as it can be seen in Fig. 4 in the case of 250k and 500k meshes.

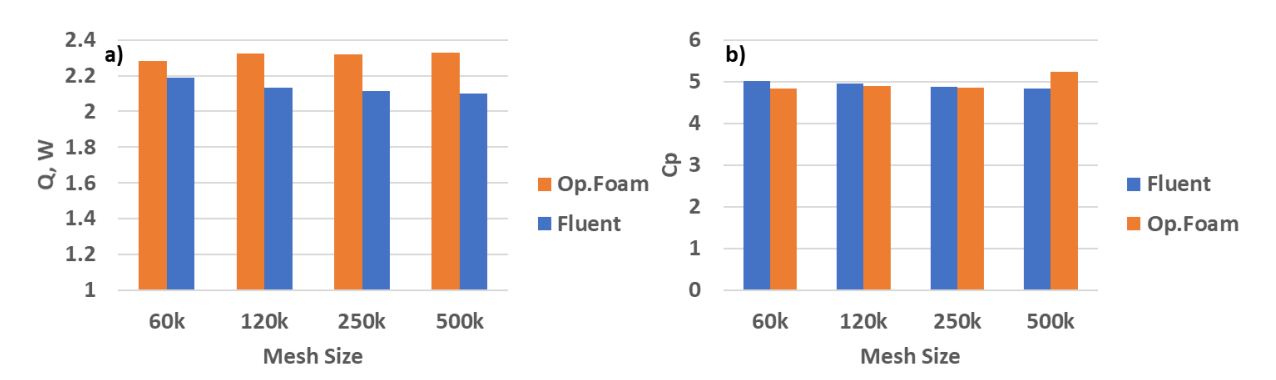


Fig. 3 a) Total heat transfer rate per unit area calculated for three different Fluent and OpenFOAM meshes.
b) static pressure coefficient for three different Fluent and OpenFOAM meshes.

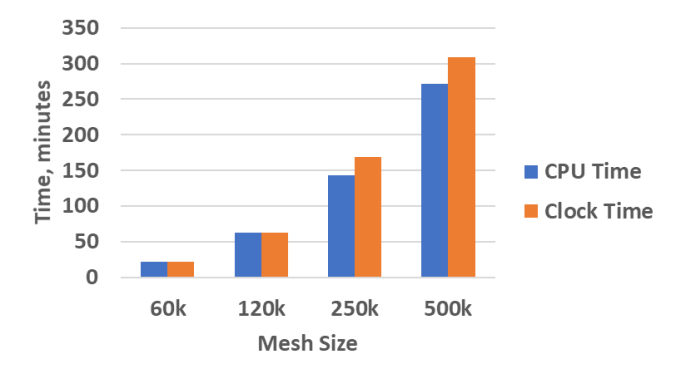


Fig. 4 CPU execution time and clock time for each OpenFOAM mesh in minutes calculated by running each simulation on the same CPU machine.

# **B.** Description of GA Procedure

There are three typical operators that are used to create new generations in a GA: crossover, mutation, and elitism. The crossover operator combines couples of parents to produce offspring. The mutation operator randomly modifies the characteristic of the offspring produced by crossover, to ensure genetic diversity. Elites are the highest performing individuals that will be directly carried over to the next generation. They are used to eliminate regression in performance from one generation to the next. This study employs another operator that is used during the selection process to determine the reproduction pool. This operator is given the term "cutoff" which is defined as the number of top performing elements that will be used as the reproduction pool for the next generation. Depending on how this number is chosen, it can include part, or all of the elites. For example, in the standard GA parameters considered in this study, the number of elites and cutoff is set to be equal. This means all of the elites are part of the reproduction pool for the next generation.

To generate new designs, the GA starts with creating the initial generation which has a total of 95 members. The rest of the standard GA parameters that were chosen for this study are listed in **Table 2**. Each member is generated by mutating the baseline geometry a random number of times between 500 (IMinM) and 5500 (IMaxM). The domain is divided into a 50x50x50 grid of voxels. A mutation is defined as randomly changing one voxel that bounds the fin, either by removing or adding it. Only border voxels are subject to mutations. For a voxel to be added it must be a fluid voxel that is adjacent to a solid voxel of the fin. For a voxel to be subtracted it must be a solid voxel that is immediately adjacent to a fluid voxel. When a mutation is invoked it first randomly determines whether the mutation will be an addition or subtraction. After this is determined, a voxel is randomly picked. If the chosen voxel fulfills the criterion for either an addition or subtraction, the mutation is finished. If not, a new voxel will be chosen and checked until this criterion is fulfilled. Constraints to prevent the attachment of fins, and formation of islands to ensure a continuous solid fin are applied. Example of the mutation process is shown in **Fig. 5**. **Fig. 6** shows the bottom view of the initial generation designs generated by mutating the baseline geometry a random number of times. In this figure and throughout this manuscript, the white space represents the solid fin body, and the black space represents the fluid domain.

The performance of each member of the initial population is evaluated in a separate CFD simulation in OpenFOAM. Since the individual evaluations are uncoupled, they are run in parallel. The metrics of interest are the total heat transfer and pressure drop for the fin domain, where the goal is to maximize heat transfer to the fluid and minimize pressure drop. The overall heat transfer is calculated from the mass flow rate and the change in mass averaged temperature from inlet to exit. Pressure drop is determined from the difference in average pressures from inlet to outlet. The presence of two objectives would normally require multi-objective optimization, but in this study a composite fitness function is optimized. The definition of fitness (F) below allows for simpler single objective optimization. Note that F is not unitless here.

$$F = \frac{Q}{dP^{1/3}} \frac{[W]}{[Pa]} \tag{1}$$

The pressure drop is raised to the 1/3 power per the methodology of Webb and Eckert [26], so that the thermal performance is evaluated for equivalent pumping power of the fluid. The designs are ranked by fitness after simulations are successfully completed. A simulation is considered complete if all the residuals of streamwise velocity, cross stream velocity, temperature, and pressure have stopped changing or are below 1x10<sup>-6</sup>. Then the elites from the design pool will be advanced directly to be part of the next generation. A "cutoff" specifies the number of designs that will get to reproduce, and any designs below the cutoff will be eliminated from the reproduction pool.

After completing the ranking, the second generation is created. The number of members that need to be created for the second generation is equal to the total population (95) minus the number of elites. There are three different mechanisms to generate new members. The first is used to generate the initial generation from the baseline geometry by simply mutating it a random number of times until all the designs are generated. The second and third mechanisms are used to generated designs after the first generation. They are similar in that they employ crossover operator to generate a child using two parent designs, and then further mutate it to increase its diversity. However, the first mechanism crosses-over a voxel only if it has the same value in both parents. More details about these mechanisms are found in [3] and will not be further discussed here. The GA will start over again by evaluating the new population in CFD followed by the selection process and crossover and mutation. Fig. 5 shows an example of the second mechanism crossover process used to produce a "child" from two "parents". These steps are repeated until an asymptotic behavior of the performance is achieved, or until a certain number of generations to limit the GA from running indefinitely.

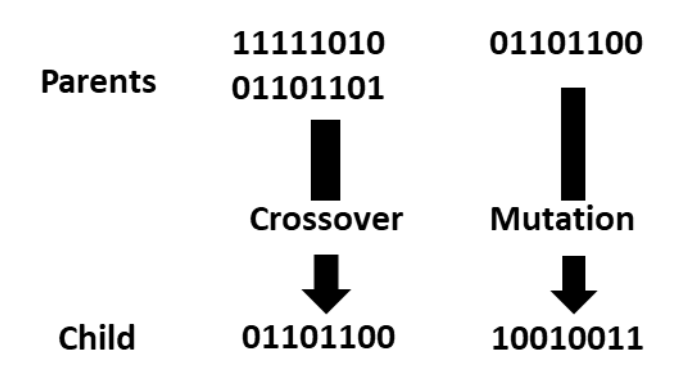


Fig. 5 Example of crossover and mutation processes used by the genetic algorithm to generate new designs.

	113		158		106		147		181		103		159		155
112.61	108	112.12	104	111.52	141	111.43	150	111.35	193	111.34	176	111.26	194	111.05	120
110.96	192	110.82	157	110.76	166	110.66	110	110.6	161	110.37	142	110.2	154	109.63	172
109.42	182	109.39	132	109.36	111	109.26	188	109.2	117	109.16	152	109.14	169	109.13	101
108.94	129	108.8	190	108.7	180	108.42	186	108.33	116	108.17	123	108.13	107	107.99	143
107.89	153	107.74	100	107.74	102	107.6	105	107.56	109	106.77	112	106.38	114	106.19	115
105.8	1118	103.47	119	0.0	121	0.0	122	0.0	124	0.0	125	0.0	126	0.0	127
0.0	128	0.0	130	0.0	131	0.0	133	0.0	134	0.0	135	0.0	136	0.0	137
0.0	138	0.0	139	0.0	140	0.0	144	0.0	145	0.0	146	0.0	148	0.0	149
0.0		0.0		0.0		0.0		0.0		0.0		0.0		0.0	167
0.0	151	0.0	156	0.0	160	0.0	162	0.0	163	0.0	164	0.0	165	0.0	
	168		170	0.0	171	0.0	173	0.0	174	0.0	175	0.0	177	0.0	178
	179		183		184		185		187		189		191		

Fig. 6 Population members of the first generation generated from the baseline geometry through the mutation process – bottom view.

**Table 2 Standard GA Parameters** 

n	Elites	Cutoff	IMaxM/IMinM
95	36	36	5500/500

# V. Results and Discussion

The GA is initially run for 60 total generations for the nominal conditions of Re = 334 (based on the hydraulic diameter) and the standard parameters in **Table 2** above, using AlSi10Mg (properties given in **Table 3**) as the solid fin material. **Fig. 7**a depicts the individual fitness, the average fitness, and the maximum fitness at each generation as a function of generation number. The limit for the number of generations was initially determined based on results from the previous 2D study (**Fig. 7**b). However, contrary to **Fig. 7**b, as the generations progress, the best and the average fitness values are still changing. This indicates that the GA will likely produce even better designs if it is run for more generations, but this was not possible at the time of writing this paper due to high computational requirements. Despite that, after 60 generations, the GA produced a geometry that performed over 18% better than the baseline rectangular fins from which the algorithm started.

Fig. 8 is a Pareto chart for the nominal GA results, with pressure drop on the horizontal axis and heat transfer on the vertical axis both normalized by their respective baseline design values, where the baseline is the rectangular fin geometry. The various designs are colored by generation number, starting with dark colors, and progressing to lighter colors toward generation number 60. The resultant population shows a clear tradeoff between pressure drop and heat transfer. The best designs all lie on the upper leftmost front of this grouping (note the location of baseline and optimal designs colored in red). In the case of Fig. 8a, which represents 3D fin results, the pressure drop for some of the optimal designs is more than 17% less than that of the baseline value while achieving heat transfer improvement up to 20% for a combined overall performance improvement of more than 18%. Fig. 8b represents the 2D results from the previous study [3], which have similar reduction in pressure drop values for a few of the optimal designs, but with heat transfer enhancement up to 55% and overall performance improvement of 60%. In addition to the aforementioned fact about the lack of asymptotic behavior in the 3D case after 60 generations, a range of assumptions to simplify the 2D case may have directly contributed to the resulting high performance-improvement. Most important of these assumptions is the 100% fin efficiency (no conjugate heat transfer). Fig. 8 also shows that the majority of designs generated in the 3D case have pressure drop value somewhat similar to the baseline value with maximum increase of ~30% and a considerable number of high performing designs with a pressure drop lower than the baseline. An interesting phenomenon in this case is that the GA tended to improve the performance by increasing the surface area (increased pressure drop) at the beginning of the optimization process and up to generation ~25. After that a clear trend of decreasing the pressure drop is observed until the end of the optimization process, leading to many optimal and semi-optimal designs with lower pressure drop as can be seen in Fig. 8a. On the other hand, the majority of generated designs in the 2D case have much higher pressure drop values compared to the baseline with maximum increase of 400% in one of the designs. This indicates that the GA was trying to maximize the fitness function by increasing the heat transfer surface area, which subsequently increases the pressure drop. Ultimately, the GA understood that striking a balance between the heat transfer enhancement and the pressure drop penalty is important to maximize the fitness function. Even though there was a single objective function, the algorithm clearly produces a range of optimal designs that would achieve high overall performance.

**Fig. 9**a shows the optimal designs for both cases (bottom view for the 3D case) along with baseline geometries. The optimal fins in the 2D case are longer and thicker than the baselines which is consistent with what was mentioned earlier about the GA tendency to maximize the fitness function by increasing the heat transfer surface area. **Fig. 9**b shows an isometric view of the optimal geometry in the 3D case along with the baseline geometry. It can be observed that the GA removed more material from the leading edge of the first fin to generate an aerodynamic shape that helps reducing the pressure drop, while adding or maintaining material elsewhere, especially in the first fin. It also appears that the GA mutates (add or remove voxels) the first fin more aggressively, suggesting that a more aggressive randomization approach is needed. More details about the hydraulic and thermal performance characteristics of this geometry is provided in the following sections.

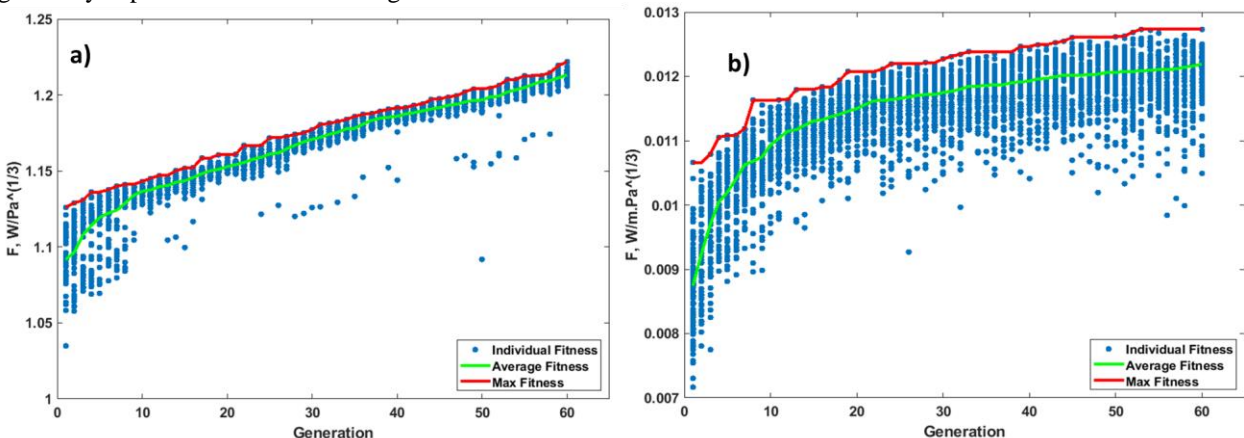


Fig. 7 The individual, average, and maximum fitness of each generation. a) 3D case. b) 2D case [3].

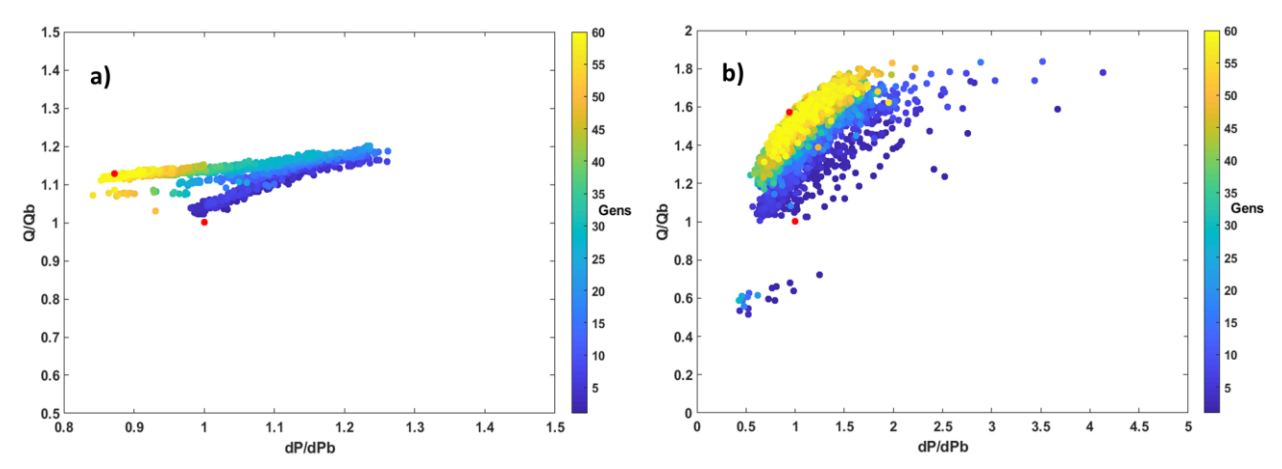


Fig. 8 Comparison of Pareto front for the nominal conditions a) 3D case. b) 2D case [3].

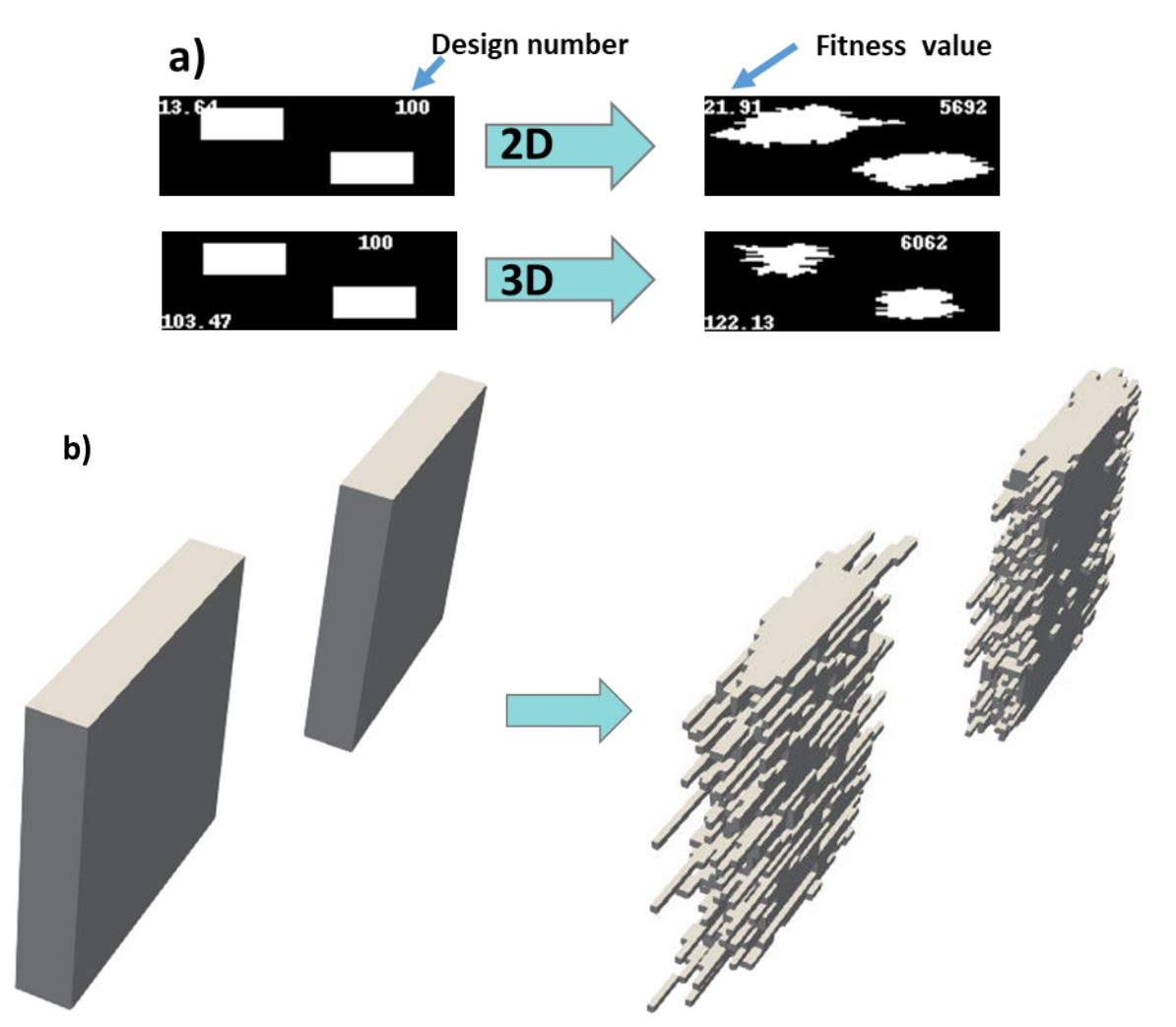


Fig. 9 a) the baseline and the resulting optimal designs for the 2D case (top) and 3D case (bottom) b) isometric view of the baseline and the resulting geometry of the 3D case after 60 generations.

# A. Effect of Fin Material

This study evaluates and compares the performance of resulting designs optimized using two heat exchanger materials: AlSi10Mg and Inconel 718. These two alloys are commonly used for additively manufactured HEXs. The

standard GA parameters settings remained similar in both cases. **Table 3** provides details of the two materials' properties relevant to the optimization process.

Table 3 Material properties for AlSi10Mg and Inconel 718 [27]

Material	Thermal Conductivity W/m².K	Specific heat, j/kg.K	Density, kg/m <sup>3</sup>
AlSi10Mg	110	915	2670
Inconel 718	12	435	8190

The resulting optimal designs have a maximum fitness improvement of 18% in the case of AlSi10Mg and 11% improvement in the Inconel 718 case. An apparent reason for the reduction in overall performance improvement in the case of Inconel 718 is the reduction in heat diffusion in the fin body due to the much lower thermal conductivity compared to AlSi10Mg. This phenomenon is demonstrated in Fig. 10 which shows the front view of temperature distribution on the fin body. In both cases the fin body temperature decreases from top and bottom towards the center, and from left to right in the streamwise direction due to heat diffusion and convection effects, respectively. However, in the case of AlSi10Mg (Fig. 10a), the temperature across the fin body is much closer to the upper and lower boundary condition which is set to a constant surface temperature of 450K. As pointed out earlier, this is due to the high thermal conductivity of AlSi10Mg. In Fig. 10b, the temperature across the fin body is much lower than the upper/lower boundaries, when compared to AlSi10Mg case. This distinction between the two cases is amplified in the overall heat transfer from the domain (important for the calculation of fitness function) which is evaluated using the average temperature at the outlet of the solid-fluid domain. Fig. 11 shows this temperature distribution at the outlet for both cases. The average outlet temperature in the case of AlSi10Mg is about 2.63K higher than the Inconel case resulting in a 3.5% higher overall heat transfer. To compensate for the low thermal conductivity in the case of the Inconel 718, the GA increased the heat transfer surface area, which resulted in higher pressure drop levels relative to the AlSi10Mg case.

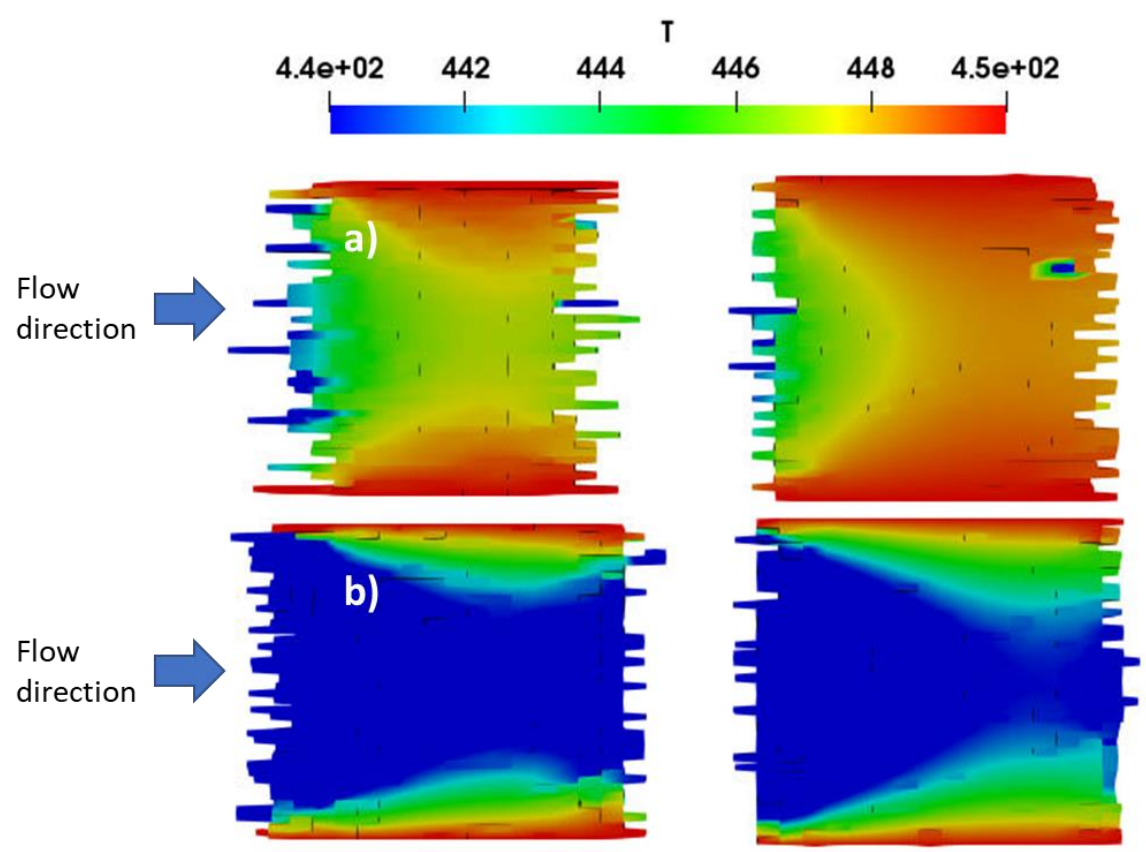


Fig. 10 Temperature distribution in the pair of fins for the optimal designs for a) AlSi10Mg b) Inconel 718.

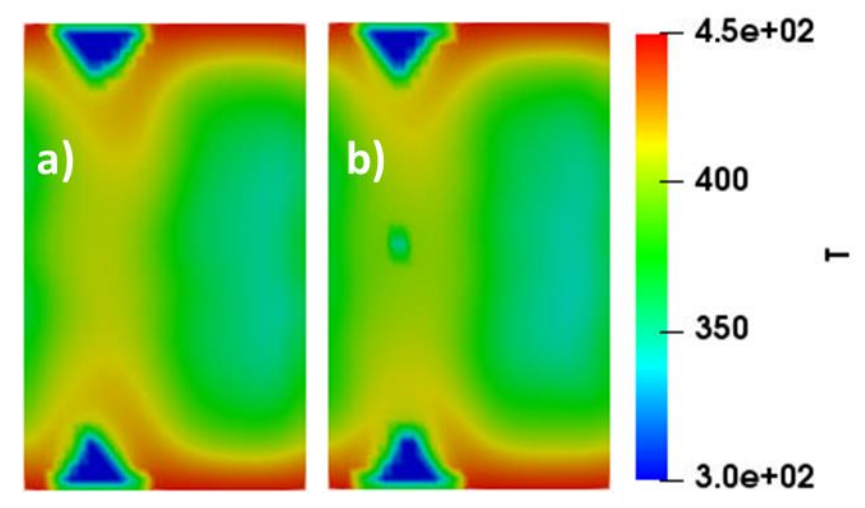


Fig. 11 Temperature distribution at the outlet of the fluid domain of a) AlSi10Mg and b) Inconel 718.

Fig. 12 shows the bottom views of the solid-fluid domain for the resulting optimal designs along with their respective fitness values plotted at the bottom left of the domain. Fig. 13 is an isometric view of the optimal fins (without the fluid domain) for both cases. These two figures clearly show that in the case of AlSi10Mg, the GA removed more material from the leading edge of the first fin and throughout the remainder of the two fin bodies which resulted in optimal designs that have more than 20% decrease in pressure drop compared to the baseline, as discussed earlier. In the case of Inconel 718 however, the GA added more surface area to enhance the heat transfer in the domain to compensate for the relatively low thermal conductivity of the fin material. This resulted in optimal designs that have pressure drop increase of more than 10% relative to the baseline, and more than 30% when compared to the optimal designs of AlSi10Mg material. These variations in pressure drop and heat transfer trends for the resulting designs from the two cases are highlighted in Fig. 14 which shows the pressure drop and heat transfer Pareto Front. The majority of the optimal designs in the AlSi10Mg case lie in the upper left front and to the left of the baseline geometry indicating lower pressure drop and higher heat transfer, which is ideally desired. The optimal designs in the case of Inconel 718 lie in the upper front and slightly to the right of the baseline. This does not necessarily mean theses designs are ineffective. The optimal designs from both cases provide significant improvement over the baseline, and their effectiveness is application dependent. For instance, aluminum and aluminum alloy (such as AlSi10Mg) heat exchangers are used in applications where thermal efficiency and the need to remove a considerable amount of heat is important. However, aluminum HEXs are limited by the maximum operating temperature. This is where HEXs made of Inconel and other high temperature tolerant alloys are more appropriate in applications such as gas turbine engines and other space related applications. Note that the thermal conductivity of the fin material is important in this analysis because the heat transfer is a major component of the defined fitness function that guide the performance of the GA. The role of thermal conductivity on the behavior of the GA could be attenuated by altering the fitness function if other properties such as density (weight) are more important to the targeted application.

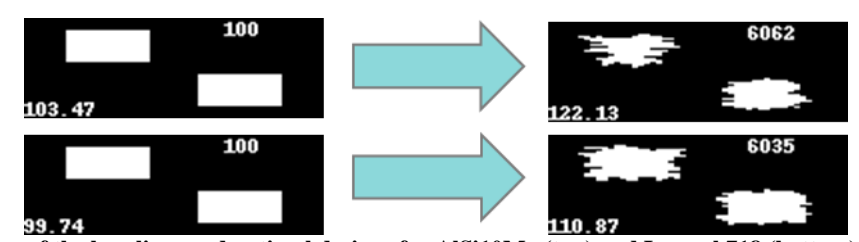


Fig. 12 Bottom view of the baselines and optimal designs for AlSi10Mg (top) and Inconel 718 (bottom) with the fitness value at the lower left corner of the solid-fluid domain and the design number on the upper right.

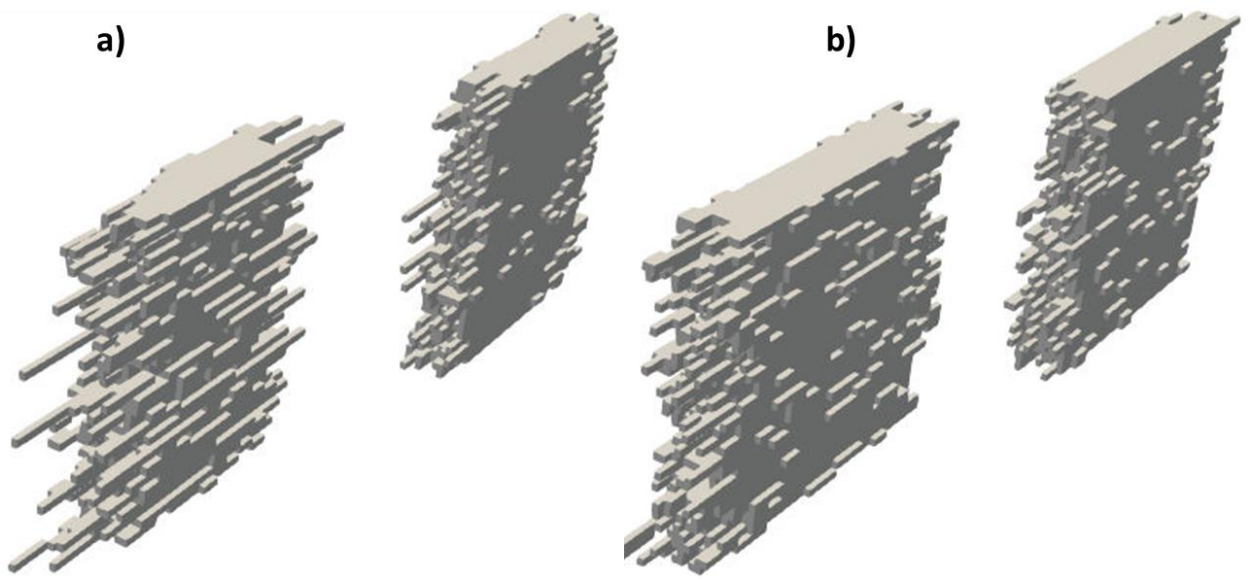


Fig. 13 shows isometric views of the optimal designs for a) AlSi10Mg and b) Inconel 718.

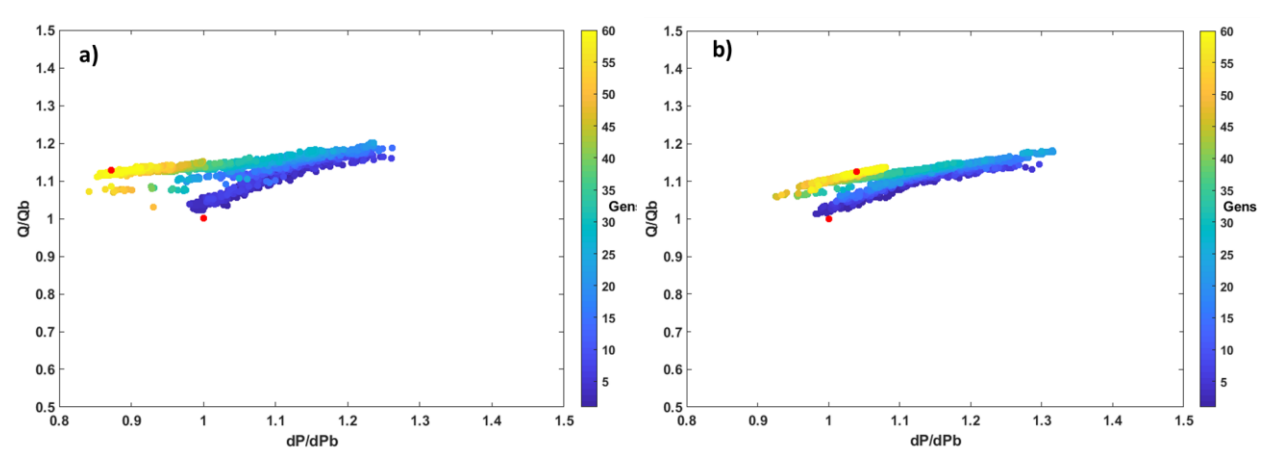


Fig. 14 The Pareto front of resulting designs for two different materials. a) AlSi10Mg b) Inconel 718.

## B. Manufacturability of Optimized Designs

The GA was developed with additive manufacturing (AM) in mind as a potential manufacturing process to build the resulting designs. AM capabilities allow for seamless digital transformation of the optimal designs. Additionally, manufacturing constraints such as the minimum build layer and bend radius can be implemented in the GA after identifying them in the targeted AM process. In the current study, the minimum voxel dimension is 0.06mm which is within the limits of what can be printed using metal AM processes [28]. However, a valid concern about the optimal designs presented here is the ability to manufacture the long extensions highlighted in **Fig. 15**. Incorporating a support structure during the build process might help manufacturing them, but the durability of such weak links in harsh operating conditions is still questionable. This issue can be overcome by implementing constraints in the GA solver to prevent the formation of such extensions from a single voxel unit in the smaller dimension (the width). A long extension with at least two voxels stacked along the width will be easy to manufacture and might result in further performance enhancement. Additionally, a Bezier curve or b-spline algorithm can be used to smooth out the sharp edges.

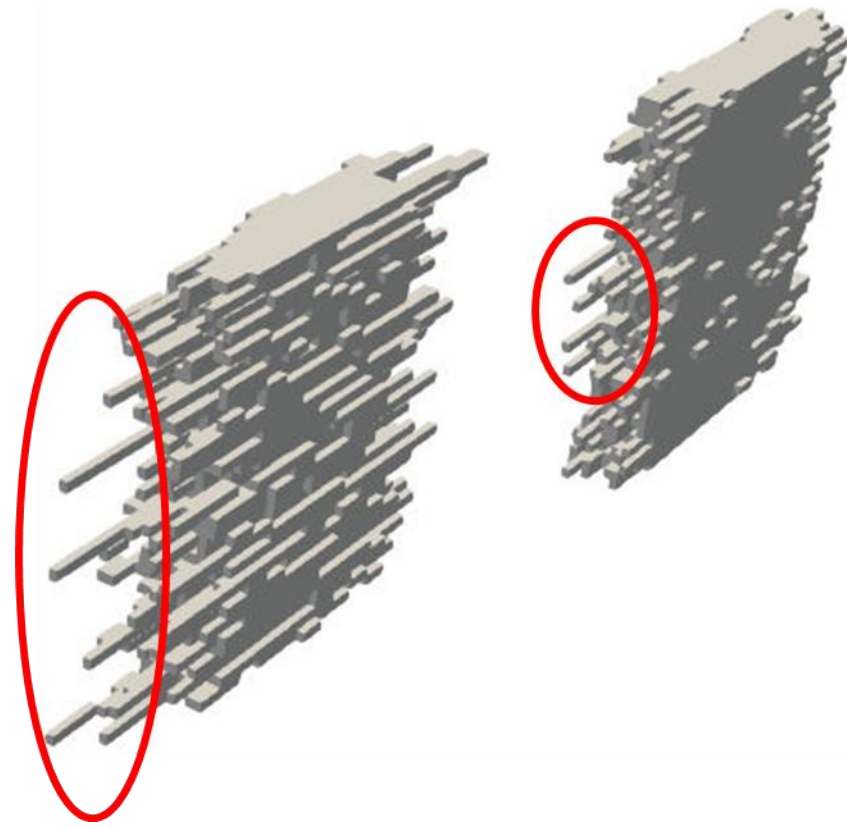


Fig. 15 An optimal design with long extensions at the leading edge highlighted.

#### VI. Conclusions

This study demonstrated the ability to produce three-dimensional (3D) non-intuitive designs using computation fluid dynamics combined with genetic algorithms and compared the results to a previously validated two-dimensional (2D) model. After 60 generations, it was found that the fitness function is still changing, suggesting that the GA might need to be run longer to determine it has reached to a global maxima. Despite that, the results showed that the optimal designs after 60 generations have overall performance improvement of 18% relative to the baseline. The optimal designs also have more than 20% reduction in pressure drop relative to their baseline compared to more than 200% increase in pressure drop in the case of 2D optimal designs relative to their baseline. Overall, the improvement level from the 3D optimization are more realistic. Concerns about the manufacturability of resulting designs can be overcome by implementing a range of smoothing techniques and manufacturing constraints.

The study also investigated the effect of varying the fin material on the resulting designs. It was found that low thermal conductivity materials lead to a lower overall performance improvement, with optimal designs that have pressure drop larger than their respective baseline designs when compared to designs produced using relatively high thermal conductivity. The definition of the fitness function should be re-evaluated when considering the effect of material properties on the overall performance.

## VII. Acknowledgements

This work was funded by the Aeronautics Research Mission Directorate (ARMD) of the National Aeronautics and Space Administration (NASA) through the NASA Fellowship Activity, under contract 80NSSC19K1683. Dr. Vikram Shyam from NASA's John H. Glenn Research Center is the technical advisor for this contract. The authors thank Ezra McNichols, Paht Juangphanich, and Brooke Weborg from NASA's John Glenn Research Center for their valuable technical contribution and feedback on this work. The authors would also like to acknowledge the use of the Pennsylvania State University's Institute for Computational and Data Sciences' Roar supercomputing system for the high-performance computing presented here.

#### VIII. References

[1] Zhang, X., Bowman, C. L., O'Connell, T. C., and Haran, K. S., 2018, "Large Electric Machines for Aircraft Electric

- Propulsion," IET Electr. Power Appl., 12(6), pp. 767–779.
- [2] NASA, 2015, "NASA Technology Roadmaps TA 15: Aeronautics," Natl. Aeronaut. Sp. Adm. [Online]. Available: https://www.nasa.gov/sites/default/files/atoms/files/2015\_nasa\_technology\_roadmaps\_ta\_15\_aeronautics.
- [3] Mekki, B. S., Langer, J., and Lynch, S., 2021, "Genetic Algorithm Based Topology Optimization of Heat Exchanger Fins Used in Aerospace Applications," Int. J. Heat Mass Transf., **170**, p. 121002.
- [4] Rodriguez, P., 1997, "Selection of Materials for Heat Exchangers," Heb, 97, pp. 1–72.
- [5] Wang, B., Klemeš, J. J., Li, N., Zeng, M., Varbanov, P. S., and Liang, Y., 2021, "Heat Exchanger Network Retrofit with Heat Exchanger and Material Type Selection: A Review and a Novel Method," Renew. Sustain. Energy Rev., 138, p. 110479.
- [6] Saltzman, D., Bichnevicius, M., Lynch, S., Simpson, T. W., Reutzel, E. W., Dickman, C., and Martukanitz, R., 2018, "Design and Evaluation of an Additively Manufactured Aircraft Heat Exchanger," Appl. Therm. Eng., 138, pp. 254–263.
- [7] Wong, M., Tsopanos, S., Sutcliffe, C. J., and Owen, I., 2007, "Selective Laser Melting of Heat Transfer Devices," Rapid Prototyp. J., 13(5), pp. 291–297.
- [8] Martin Philip Bendsoe, and Noboru Kikuchi, 1988, "Generating Optimal Topologies in Structural Design Using a Homogenization Method," Comput. Methods Appl. Mech. Eng., 71, pp. 197–224.
- [9] Borrvall, T., and Petersson, J., 2001, "Topology Optimization Using Regularized Intermediate Density Control," Comput. Methods Appl. Mech. Eng., 190(37–38), pp. 4911–4928.
- [10] Wang, M. Y., Wang, X., and Guo, D., 2003, "A Level Set Method for Structural Topology Optimization," Comput. Methods Appl. Mech. Eng., 192(1–2), pp. 227–246.
- [11] Allaire, G., Jouve, F., and Toader, A. M., 2004, "Structural Optimization Using Sensitivity Analysis and a Level-Set Method," J. Comput. Phys., **194**(1), pp. 363–393.
- [12] Norato, J. A., Bendsøe, M. P., Haber, R. B., and Tortorelli, D. A., 2007, "A Topological Derivative Method for Topology Optimization," Struct. Multidiscip. Optim., 33(4–5), pp. 375–386.
- [13] Takezawa, A., Nishiwaki, S., and Kitamura, M., 2010, "Shape and Topology Optimization Based on the Phase Field Method and Sensitivity Analysis," J. Comput. Phys., **229**(7), pp. 2697–2718.
- [14] Høghøj, L. C., Nørhave, D. R., Alexandersen, J., Sigmund, O., and Andreasen, C. S., 2020, "Topology Optimization of Two Fluid Heat Exchangers," Int. J. Heat Mass Transf., **163**, p. 120543.
- [15] Feppon, F., Allaire, G., Dapogny, C., and Jolivet, P., 2020, "Topology Optimization of Thermal Fluid–structure Systems Using Body-Fitted Meshes and Parallel Computing," J. Comput. Phys., 417, p. 109574.
- [16] Skinner, S. N., and Zare-Behtash, H., 2018, "State-of-the-Art in Aerodynamic Shape Optimisation Methods," Appl. Soft Comput. J., 62, pp. 933–962.
- [17] Sigmund, O., 2011, "On the Usefulness of Non-Gradient Approaches in Topology Optimization," Struct. Multidiscip. Optim., **43**(5), pp. 589–596.
- [18] Aage, N., Andreassen, E., Lazarov, B. S., and Sigmund, O., 2017, "Giga-Voxel Computational Morphogenesis for Structural Design," Nature, **550**(7674), pp. 84–86.
- [19] Safonov, A. A., 2019, "3D Topology Optimization of Continuous Fiber-Reinforced Structures via Natural Evolution Method," Compos. Struct., 215, pp. 289–297.
- [20] Wei, G., 2003, "An Improved Fast-Convergent Genetic Algorithm," *Proceedings of the 2003 IEEE. International Conference on Robotics, Intelligent Systems and Signal Processing*, pp. 1197–1202.
- [21] Fabbri, G., 1997, "A Genetic Algorithm for Fin Profile Optimization," Int. J. Heat Mass Transf., 40(9), pp. 2165–2172.
- [22] Liu, C., Bu, W., and Xu, D., 2017, "Multi-Objective Shape Optimization of a Plate-Fin Heat Exchanger Using CFD and Multi-Objective Genetic Algorithm," Int. J. Heat Mass Transf., 111, pp. 65–82.
- [23] Xu, G., Zhuang, L., Dong, B., Liu, Q., and Wen, J., 2020, "Optimization Design with an Advanced Genetic Algorithm for a Compact Air-Air Heat Exchanger Applied in Aero Engine," Int. J. Heat Mass Transf., 158, p. 119952.
- [24] Ha, M. Y., and Jung, M. J., 2000, "A Numerical Study on Three-Dimensional Conjugate Heat Transfer of Natural Convection and Conduction in a Differentially Heated Cubic Enclosure with a Heat-Generating Cubic Conducting Body," Int. J. Heat Mass Transf., **43**(23), pp. 4229–4248.
- [25] "5.2 Thermophysical Models" [Online]. Available: https://www.openfoam.com/documentation/user-guide/5-models-and-physical-properties/5.2-thermophysical-models. [Accessed: 18-Nov-2021].
- [26] Webb, R. L., and Eckert, E. R. G., 1972, "Application of Rough Surfaces to Heat Exchanger Design," Int. J. Heat Mass Transf., **15**(9), pp. 1647–1658.
- [27] Thole, K. A., Lynch, S. P., and Wildgoose, A. J., 2021, "Review of Advances in Convective Heat Transfer Developed through Additive Manufacturing," *Advances in Heat Transfer*, Academic Press.
- [28] "Concept Laser\_M2 Series 5\_Machine | GE Additive" [Online]. Available: https://www.ge.com/additive/additive-manufacturing/machines/m2series5. [Accessed: 18-Nov-2021].